Inter-annual variability in phytoplankton and nutrients in the Gulf of Elat/Aqaba

Hadar Berman[1], Hezi Gildor[1], Erick Fredj[2]

[1]Institute of Earth Sciences, The Hebrew University, Edmond J. Safra Campus, Givat Ram, Jerusalem 91904, Israel
[2]Jerusalem College of Technology, Department of Computer Science, 21 Haavad Haleumi St., P.O. Box 16031, Jerusalem 91160, Israel

Key Points:

- Mixed layer deepening causes horizontal advection effect on northern Gulf integrated phytoplankton to increase.
- Deep mixing causes increase in light limitation on growth in northern Gulf.
- Nutrient accumulation in the deep water is driven mostly by physical processes immediately after mixing.

Corresponding author: Hadar Berman, hadarberman@gmail.com

Abstract

The Gulf of Elat/Aqaba exhibits high inter-annual variability in mixed layer depth. Observations from the northern Gulf show differences of hundreds of meters in winter mixing depth, which ranges between 300 m in years with shallow mixing and up to 700 m in years with deep mixing. Deep mixing events can occur in two consecutive years or after four consecutive years of shallow mixing. The mixing depth has an effect on the concentration of nutrients and chlorophyll (and other tracers) in the surface and deep water. Using a 3D coupled physical-ecological model, we study the effect of shallow vs. deep mixing on the processes controlling the phytoplankton bloom and on nutrient accumulation in the deep water. We found that years with deep mixing are characterized by larger spatial variability in surface and integrated chlorophyll concentration during the mixing season. We also found that horizontal advection is more important for integrated phytoplankton concentration in years with deep mixing in the northern Gulf. Even when mixing was deep and nutrient limitation decreased, light limitation on growth was enhanced more in the north compared with the south. In addition, we showed that the nutrient accumulation in the deep water after a year with deep mixing of the northern Gulf was initially affected mostly by physical processes (such as advection and vertical mixing), and less from ecological regeneration and switched gradually to be dominated by ecological processes alone during the third year of shallow mixing.

Plain Language Summary

Primary production by phytoplankton is the base of the marine ecological system and is an important mechanism for the sequester of carbon from the atmosphere and into the ocean. In this work, we study the effect of varying mixed layer depths on the mechanisms for the phytoplankton bloom initiation, a phenomenon of increased phytoplankton concentration. We study the Gulf of Elat/Aqaba, a relatively small basin, which exhibits years of shallow and very deep mixing, as well as changing magnitudes of phytoplankton blooms. We found that deep mixing causes increased spatial variability between the northern and southern Gulf of phytoplankton concentration, both in the surface water and in the integrated column. Increase in mixed layer depth causes an increase in the effect of horizontal advection on the phytoplankton concentration in the whole water column in the northern Gulf. In addition, it causes light limitation on growth to increase in the northern Gulf, even though nutrients are more abundant after deep mixing. Finally, we show that nutrient accumulation in the deep water of the northern Gulf after deep mixing, which decreases their concentration in depth, is initially mostly due to physical processes of mixing and advection, but in the third year of shallow mixing is dominated by ecological regeneration.

1 Introduction

The Gulf of Elat/Aqaba (hereinafter **the Gulf**, Figure 1) is a small elongated (180 km X 5-25 km) semi-enclosed basin connected to the Red Sea through the relatively shallow (maximum depth ∼250 m) Straits of Tiran. Relatively warm Red Sea surface water enters through the straits during the months after mixing and replaces the Gulf's surface water (Biton & Gildor, 2011b). The deep water is formed in the northern Gulf by convection processes in shallow shelves and in the open-water (Wolf-Vecht et al., 1992; Genin et al., 1995; Biton et al., 2008) causing the temperature difference between the surface and deep water to be small compared with other ocean basins at similar latitudes (see Figure 2 upper panel). The weak stratification associated with the small temperature difference breaks every winter and results in mixing that can reach down to ∼700 m during years of very deep mixing, and down to ∼300 m during years of relatively shallow mixing.

Most of our knowledge of the Gulf's seasonal and inter-annual variability is based on monthly observations conducted in the northern tip of the Gulf (Station A, Figure 1) by the National Monitoring Program (**NMP**). These observations include vertical profiles of temperature, salinity, Photosynthetically Active Radiation (**PAR**), chlorophyll, zooplankton, nutrients, oxygen and more. Observations with higher temporal resolution of surface chlorophyll and Sea Surface Temperature (**SST**) are observed daily at a fixed location on the pier of the Underwater Observatory of Elat (coordinates: $29^o30'13.5"$N, $34^o55'3.5"$E; Figure 1), which is approximately in the same latitude as Station A, but in shallow water close to shore.

Deep mixing in the Gulf (>500 m) does not occur every year and not at regular intervals (Figure 2). Deep mixing can occur in two consecutive years (as in 2005 and 2006) or four years of shallow mixing can pass until deep mixing occurs again (2008-2012). The mixing depth has an effect both on chlorophyll and on nutrients (Figure 2 middle and lower panels). During mixing, chlorophyll and nutrient concentration are nearly constant throughout the mixed layer. Thus, mixing causes nutrients to increase in the surface water and decrease in depth. The NMP observations (Figure 2 middle panel) reveal that phytoplankton varies seasonally in the Gulf with low surface concentrations in summer during stratification, high surface and integrated concentration in winter during vertical mixing and a surface spring bloom after mixing ceases (e.g. Genin et al., 1995; Zarubin et al., 2017).

The Gulf is oligotrophic due to its input of oligotrophic northern Red Sea water through the Straits of Tiran. Since nutrients are scarce, surface and integrated phytoplankton growth in the Gulf are highly dependent on nutrient availability (Zarubin et al., 2017; Berman & Gildor, in press; Meeder, 2012). The limiting nutrient for phytoplankton growth in the Gulf is nitrogen (Levanon-Spanier et al., 1979) or a co-limitation of nitrogen and phosphorous (Suggett et al., 2009). Due to the Gulf's oligotrophic conditions, vertical mixing (manifested in the Mixed Layer Depth (**MLD**)) has an important role in injecting nutrients to the photic zone during winter (Zarubin et al., 2017; Genin et al., 1995; Meeder, 2012; Berman & Gildor, in press). While deeper mixing increases the amount of nutrients in the MLD, when the MLD is too deep it can decrease the amount of light available for primary production. Since both nutrient supply and light availability control phytoplankton growth, deeper mixing can either cause an increase or decrease in phytoplankton growth (e.g. Sverdrup, 1953; Behrenfeld & Boss, 2018; Meeder, 2012; Zarubin et al., 2017). The enhanced nutrient injection, due to the deeper vertical mixing, has been associated with enhanced surface phytoplankton spring blooms (Genin et al., 1995).

The inter-annual variability in MLD has an effect on the nutrients in the deep water of the northern Gulf. This is due to its distribution over the whole water column and its consumption in the photic zone. NMP observations show that after a deep mixing event, it takes a few years of shallow mixing for the nutrient concentration in the deep water to reach high values again ($>5\ mmol-N/m^3$) (Figure 2 lower panel). Here we studied how physical (e.g. horizontal advection and mixing) and ecological (e.g. remineralization) processes affect the accumulation of nutrients in the deep water.

Spatial variability of vertical mixing in the Gulf results in increased stratification in the southern compared with the northern Gulf (Paldor & Anati, 1979; Berman & Gildor, in press). Its effect on surface and integrated phytoplankton concentration was recently studied by Berman and Gildor (in press), and found to cause opposite gradients for the surface (from south to north) and integrated (from north to south) phytoplankton concentration. Consequently, light limitation on phytoplankton growth varies throughout the Gulf, exhibiting a higher limitation for the integrated phytoplankton in deeper mixed areas, i.e. in the northern end. The southern Gulf, which is more stratified, also exhibits light limitation, but this is not as pronounced as in the north. Horizontal advection is

a crucial process during winter in the deep mixed northern Gulf for increasing integrated phytoplankton concentration (Berman & Gildor, in press).

Here, we examine how the inter-annual variability in mixing depth affects the spatial variability of phytoplankton and nutrient concentration. This is done using a 3D coupled physical-ecological model, simulating two consecutive years of shallow (2011) and deep (2012) mixing. We also simulated five consecutive years, one of shallow mixing, one of deep mixing and three more years of shallow mixing, to study the nutrient accumulation in the deep water after intense mixing. Our main findings are: (1) deepening of the MLD in years of very deep mixing is enhanced more in the northern Gulf compared with the south; (2) for integrated phytoplankton, the importance of horizontal advection is enhanced in a year with deep mixing (3) even when mixing is deep and nutrient limitation decreases, light limitation on growth is enhanced more in the north compared with the south; (4) nutrient accumulation in depth is driven more by physical processes in the first year after mixing. However, during the third year of shallow mixing, ecological processes govern the accumulation.

The paper is organized as follows: Section 2 details the model configuration including the physical model (Subsection 2.1), the ecological model (Subsection 2.2), the optimization procedure (Subsection 2.3) and comparison of model results to independent observations (Subsection 2.4). Calculations are detailed in Section 3, results in Section 4 and discussion in Section 5.

2 Model configuration and results

2.1 Physical model

The physical model for climatological conditions, implemented using The Massachusetts Institute of Technology General Circulation Model (**MITgcm,** Marshall, Adcroft, et al., 1997; Marshall, Hill, et al., 1997), was previously used to study dynamical processes in the Gulf (Biton & Gildor, 2011c, 2011a, 2011b, 2016). The model's domain (Figure 1) includes the whole Gulf, ending 20 km south of the Straits of Tiran. Horizontal resolution is 300 m with 32 vertical levels concentrated mostly in the upper 300 m. The model is a free-surface, hydrostatic primitive equation ocean model with a KPP mixing scheme (Large et al., 1997) suitable for unstable regimes. The horizontal viscosity is calculated using Smagorinsky scheme (Smagorinsky, 1963). There is no explicit horizontal diffusion, but tracer's horizontal eddy diffusivity is indirectly influenced by the advection scheme. Net evaporation, heat flux and wind stress were used as surface boundary conditions as well as relaxation to SST and sea surface salinity (details on the forcing can be found in Biton & Gildor, 2011b). An open boundary for the Straits of Tiran is used to relax temperature and salinity to climatological profiles (more information in Biton & Gildor, 2011b).

Here, we altered the climatological model described above (Biton & Gildor, 2011b) to simulate inter-annual variability for two consecutive years with shallow (down to ∼300 m) and deep (down to ∼700 m) mixing. The simulation of the year of shallow mixing runs between 1/12/2010-30/11/2011 and will be referred to as **2011, year of shallow mixing**. The simulation of the year of deep mixing runs between 1/12/2011-30/11/2012 and will be referred to as **2012, year of deep mixing**. These specific years were simulated by using two specific forcing: (1) wind speed at 10 m every three hours (derived from a regional atmospheric model - see Appendix 1 for more details) and (2) relaxation of three days to SST derived from the Moderate Resolution Imaging Spectroradiometer (MODIS) instrument aboard the Aqua and Terra satellites of 9 km and 8-day average products (obtained from `https://oceancolor.gsfc.nasa.gov/`). For simplicity, we used MODIS SST value in the north and south and linearly interpolated between them. The data was then

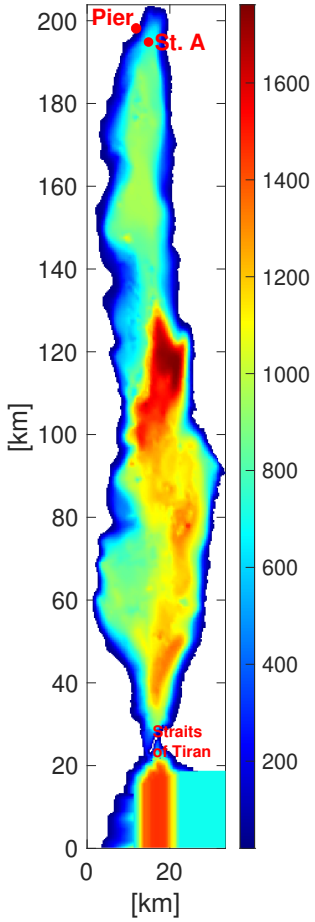

Figure 1. Model domain and the bathymetry of the Gulf. Water enters the Gulf from the Red Sea through the Straits of Tiran. The location of Station A and the pier of the Underwater Observatory of Elat in the north, where monthly and daily (respectively) observations from the National Monitoring Program (**NMP**) are taken, is shown. For more information see Section 1.

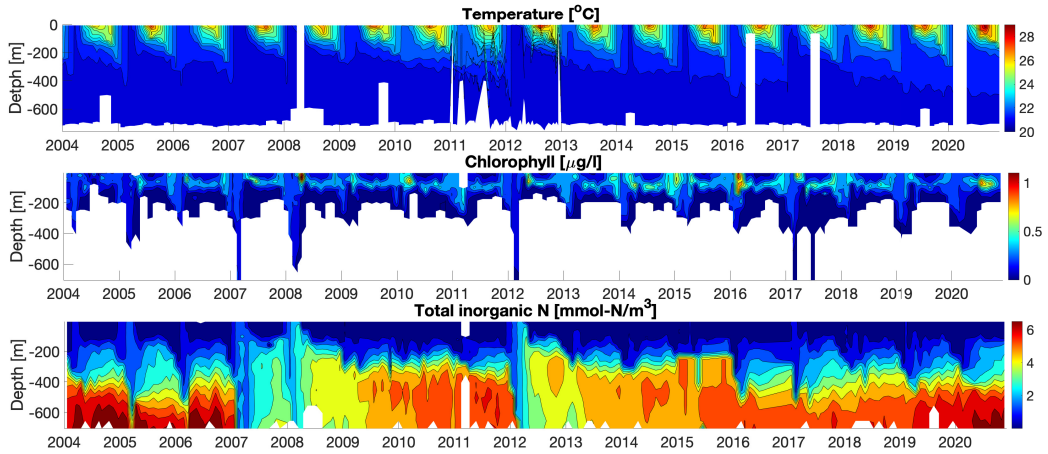

Figure 2. Time series depth profiles of temperature (upper panel, $[^oC]$) chlorophyll (middle panel, $[\mu g/l]$) and total inorganic nitrogen (lower panel, $[mmol\text{-}N/m^3]$) between 2004-2020, based on monthly casts in Station A observed by the NMP.

linearly interpolated from 8 days to hourly resolution. A 20 day spin-up was conducted with realistic initial conditions. Other forcing, boundary conditions and model details have not been changed from the original climatological model (Biton & Gildor, 2011b).

Figures 3 and 4 show the physical model daily mean results corresponding to the once-a-month NMP observations for the two specific years of 2011 and 2012 respectively. Overall, the model reproduces the observed temperature and MLD profiles rather well. We note that tidally-driven internal waves are not accounted for in the model. It was shown before that the amplitude of tidally-driven internal waves is a few tens of meters (see Figure 6 in Carlson et al., 2014). As the NMP profiles were taken at a specific time (and phase) of the internal waves, some differences between the observations and the simulation are expected. The MLD deepens from December 2010 until March 2011 when it reaches its maximum of ∼300 m, i.e. a winter with relatively shallow mixing. Stratification begins in April (temperature profile is not a straight line anymore) and continues until October, when mixing starts again (Figure 3). The maximum SST of the model is lower than that observed in the summer months (∼25°C and ∼26°C in August for model and NMP respectively). The modeled SST in summer shows differences from NMP observations since surface heat flux of the model has not been change from the climatological conditions and has a large effect on surface SST. Heat fluxes have not been changed from the climatological conditions since they produced the best fit to the MLD in the different years, which was more important to simulate than the surface temperature. The MLD deepens in the winter of 2012 (Figure 4) until March when a maximum MLD of 700 m is reached in both model and NMP. Stratification starts in April and continues until October, when mixing starts again.

Figure 5 shows a comparison of the model upper layer temperature to SST satellite imagery by MODIS-AQUA level 3 (obtained from https://oceancolor.gsfc.nasa.gov/l3/) for the stratified and mixed season of 2011 and 2012. The comparison is done on the model upper layer which is 10 m thick since SST from the satellite are skin retrievals (as detailed in `https://modis.gsfc.nasa.gov/data/atbd/atbd_mod25.pdf`). The cold temperatures in

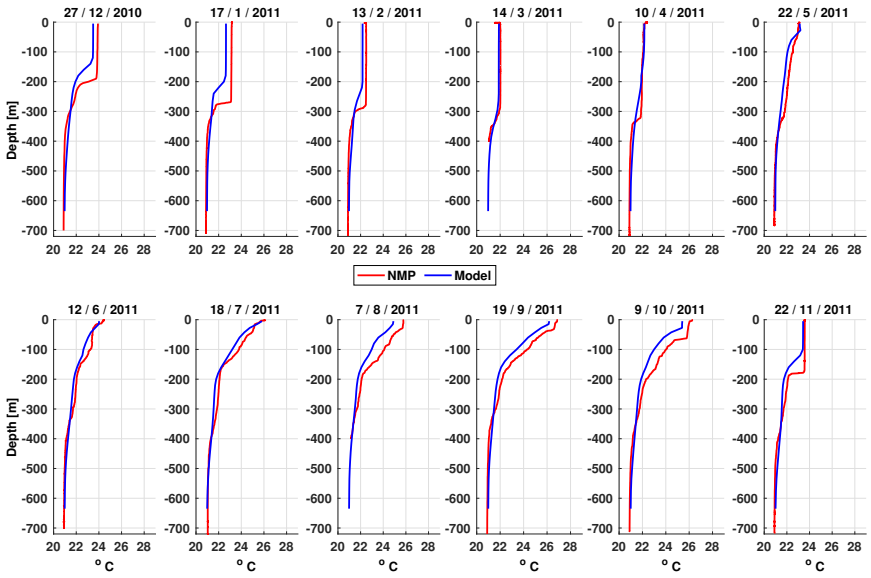

Figure 3. Observed (red) and simulated (blue) temperature profiles in 2011. Observations are measured once a month by the NMP in Station A. The simulated profiles are daily means from a grid point closest to Station A in the same date of the NMP cruise of that month.

winter and the warmer temperatures in summer, as well as the east to west temperature gradient in summer, can be seen both by MODIS and by the model results. Modeled summer SST is lower in some parts of the Gulf compared to MODIS imagery.

2.2 Ecological model

The ecological model is a simplified Nutrient-Phytoplankton-Zooplankton-Detritus (NPZD) model, including one Phytoplankton (P, $[mmol\text{-}N/m^3]$) and Zooplankton species (Z, $[mmol\text{-}N/m^3]$), Nitrogen as the limiting nutrient (N, $[mmol\text{-}N/m^3]$) and Detritus (D, $[mmol\text{-}N/m^3]$). In addition, there is an equation to convert phytoplankton biomass to chlorophyll (CHL, $[\mu g/l]$), following Geider et al. (1997). The equations are based on Follows et al. (2007), but were altered to include processes shown to be significant in the Gulf.

The model equations are given in Equations 1-5. The left hand is composed of the material derivative $\frac{D}{Dt} = \frac{\partial}{\partial t} + \vec{V}\vec{\nabla}$. The right-hand side describes the ecological processes and vertical mixing. K is the vertical eddy mixing coefficient derived from the KPP mixing scheme.

$$\frac{DN}{Dt} = -\mu \frac{N}{N + k_{satN}} i_{lim} P + k_{min} D + m_{zn} Z + m_{pn} P + \frac{\partial}{\partial z}(K \frac{\partial N}{\partial z}) \quad (1)$$

$$\frac{DP}{Dt} = \mu \frac{N}{N + k_{satN}} i_{lim} P - g \frac{P^2}{P^2 + k_{gsat}^2} Z - m_p P - m_{pn} P + \frac{\partial}{\partial z}(K \frac{\partial P}{\partial z}) \quad (2)$$

$$\frac{DZ}{Dt} = e_{eff} g \frac{P^2}{P^2 + k_{gsat}^2} Z - m_{zn} Z - m_z Z^2 + \frac{\partial}{\partial z}(K \frac{\partial Z}{\partial z}) \quad (3)$$

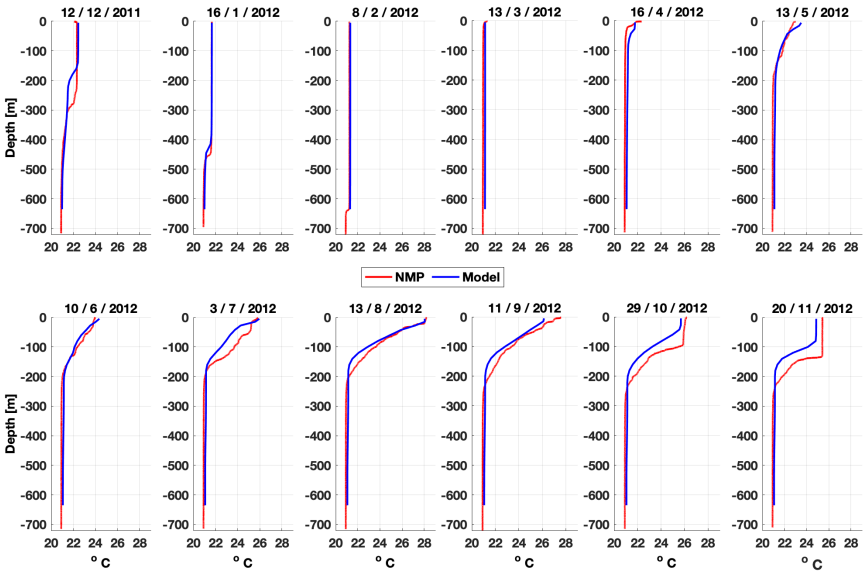

Figure 4. Observed (red) and simulated (blue) temperature profiles in 2012. Observations are measured once a month by the NMP in Station A. The simulated profiles are daily means from a grid point closest to Station A in the same date of the NMP cruise of that month.

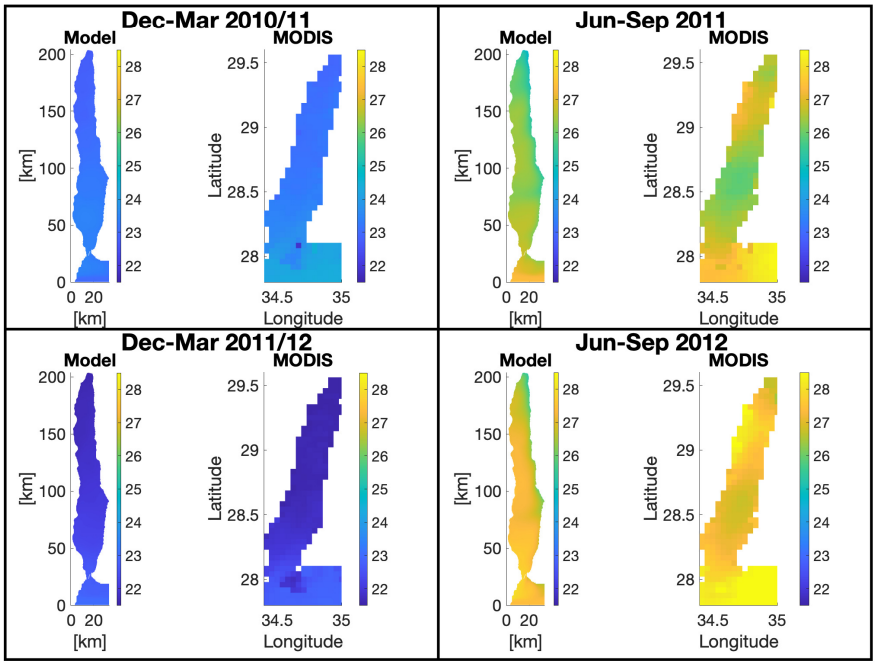

Figure 5. SST as observed by MODIS-AQUA level 3 imagery compared with monthly mean SST of the model for the stratified season (July-September) and mixed season (December-March) in 2011 and 2012.

Table 1. Parameters of the NPZD model. The first 13 parameters were optimized within the ranges found in literature. The optimized value is specified in the last column. The two constrained parameters measured specifically for the Gulf are detailed in the last two rows.

Param	Units	Parameter explanation	Range	Ref	Best fit
k_{min}	d^{-1}	Remineralization rate	0.003-0.15	[a,b]	0.0042
m_{zn}	d^{-1}	Z excretion rate	0.01-0.35	[c,d]	0.066
μ	d^{-1}	P maximum growth rate	0.2-3	[b,e]	0.59
k_{satN}	$mmol\text{-}Nm^{-3}$	N half saturation coefficient	0.01-3.5	[d,e]	0.35
g	d^{-1}	Maximum grazing rate	0.1-4	[c,d,e]	3.5
k_{gsat}	$mmol\text{-}Nm^{-3}$	Grazing half saturation coefficient	0.1-5	[c,d,e]	1.6
m_p	d^{-1}	P mortality rate	0.01-0.25	[d]	0.02
m_{pn}	d^{-1}	P respiration rate	0.005-0.25	[d]	0.037
m_z	$(mmol\text{-}Nm^{-3})^{-1}d^{-1}$	Z mortality rate	0.01-1	[b]	0.97
e_{eff}	non-dimensional	Grazing efficiency	0.5-1		0.76
w_{ns}	md^{-1}	PON sinking rate	0.0024-20	[e]	0.2
α_{chl}	$mmol\text{-}N\mu g\text{-}chl^{-1}$ $m^2\mu E^{-1}$	Initial slope of the PI curve normalized to chlorophyll	$(0.18\text{-}3.15)\cdot 10^{-7}$	[f]	$0.77\cdot 10^{-7}$
θ_m	$\mu g{-}chl\cdot mmol\text{-}N^{-1}$	Maximum chlorophyll to N ratio	0.4-5.72	[f]	2.1
k_c	$m\cdot mg\text{-}chl^{-1}$	Light attenuation due to P	$6.7\cdot 10^{-4}$	[g]	-
k_0	m^{-1}	Clear-water attenuation coefficient	0.04	[h]	-

[a]Follows et al. (2007)
[b]Schartau and Oschlies (2003)
[c]Kuhn et al. (2018)
[d]Kuhn et al. (2015)
[e]Evans and Garçon (1997, chapter 8)
[f]Geider et al. (1997)
[g]Dishon et al. (2012)
[h]Stambler (2006)

$$\frac{DD}{Dt} = m_pP + m_zZ^2 - k_{min}D + (1-e_{eff})g\frac{P^2}{P^2+k_{gsat^2}}Z + w_{ns}\frac{\partial D}{\partial z} + \frac{\partial}{\partial z}(K\frac{\partial D}{\partial z}) \quad (4)$$

$$\frac{DCHL}{Dt} = \rho_{chl/phy}\mu\frac{N}{N+k_{satN}}i_{lim}P - m_pCHL - g\frac{P^2}{P^2+k_{gsat^2}}Z\frac{CHL}{P} - m_{pn}CHL + \frac{\partial}{\partial z}(K\frac{\partial CHL}{\partial z}) \quad (5)$$

The ecological model includes 13 free parameters and two constrained parameters which were measured in for the Gulf as detailed in Table 1. The 13 free parameters were bounded between ranges found in the literature as detailed in the reference column of Table 1 and optimized to their final values (see Section 2.3).

Light attenuation was modeled as $PAR(z) = PAR(0)e^{(k_0+k_cChl)z}$, (similar to Follows et al., 2007) where z is depth [m], $PAR(z)$ and $PAR(0)$ are the PAR in depth z and depth $z = 0$ and Chl is the total chlorophyll concentration above

depth z in units of $mg\text{-}chl/m^2$. The two constrained model parameters based on measurements in the Gulf are related to light attenuation: (1) the minimum light attenuation coefficient in the Gulf k_0 (Stambler, 2006), and (2) chlorophyll self shading coefficient k_c (Dishon et al., 2012).

Nutrient limitation on growth was modeled as a Michaelis-Menten kinetics. The nutrient limited growth is therefore $Pm = \mu \frac{N}{N+k_{satN}}$. Light limitation effect on phytoplankton growth ($ilim$, e.g. in Equation 2) was modeled as $ilim = (1 - exp(-\alpha_{chl} PAR\theta/Pm))$ (Geider et al., 1997, adapted from Equation 1). Here θ is the ratio between chlorophyll and phytoplankton ($\theta = \frac{CHL}{P}$) and α_{chl} is the initial slope of the photosynthesis-irradiance (PI) curve normalized to chlorophyll concentration, which determines the rate of photosynthesis in low light intensities (see Table 1).

Phytoplankton loss is represented by two terms, mortality ($m_p P$) and respiration ($m_{pn} P$). The mortality term ($m_p P$) transfers matter directly to the detritus pool (and indirectly to the nitrogen pool). The respiration term ($m_{pn} P$) transfers matter directly to the nitrogen pool, as has been done for the Atlantic Ocean (Fennel et al., 2001).

Zooplankton grazing was modeled as a Holling type III function, which is commonly used in similar models. This function simulates grazing as increasing rapidly in low density prey, and slowing down at higher prey densities until grazing reaches saturation (e.g. Schartau & Oschlies, 2003; Kuhn et al., 2015, 2018). Zooplankton loss due to higher predators (closure term) was divided into two parts. The first is death rate, modeled as a quadratic term. The quadratic form was used in the past for the Gulf and for the Atlantic Ocean (Kuhn et al., 2018; Fennel et al., 2006) and causes higher death rates at higher zooplankton concentrations compared with the linear case (Franks, 2002). The second is a linear loss term of zooplankton nitrogen excretion ($m_{zn} Z$), important for the nitrogen cycle (Capone et al., 2008, chapter 3). It has been used by Kuhn et al. (2015, 2018) for the Atlantic Ocean and for the Gulf.

The chlorophyll equation (Equation 5) was based on Equation 3 in Geider et al. (1997), which converts phytoplankton biomass to chlorophyll. As in Geider et al. (1997), $\rho_{chl/phy}$, the ratio of chlorophyll synthesis to carbon fixation (or phytoplankton increase), and is modeled as $\rho_{chl/phy} = \frac{\theta_m \mu \frac{N}{N+k_{satN}} i_{lim} P}{\alpha_{chl} \cdot PAR \cdot CHL}$. Here θ_m is the maximum chlorophyll to N ratio (as detailed in Table 1).

Forcing

The ecological model in the surface was forced by PAR. Hourly data of surface PAR were downloaded from IUI meteorological data (`http://www.meteo-tech.co.il/eilat-yam/eilat_download_en.asp`) in the period of 1/12/2010 - 30/11/2012 and averaged daily. Resolving the diurnal cycle did not change significantly the model correspondence to observations, as the parameters of the model change respectively to achieve a better fit to observations.

The southern boundary of the model is relaxed to nitrate climatological observations from the northern Red Sea Station 28862 downloaded from the WOA13 (`https://www.nodc.noaa.gov/cgi-bin/OC5/woa13/woa13oxnu.pl`). Relaxation time for the boundary condition is one day. This is the only open boundary in the model, i.e. there is no accumulation of matter in the sediments.

Initial conditions

All variables were initialized based on NMP data of 1st December 2010. Nitrogen was initialized from combined data of nitrite and nitrate. Phytoplankton is based on chlorophyll data from the NMP. Phytoplankton was converted from chlorophyll units ($\mu g/l$) by using a value of 40 $mg\text{-}C/mg\text{-}Chl$ (Zarubin et al., 2017), the Redfield ratio and carbon molecular weight to get units of $mmol\text{-}N/m^3$. The conversion for the initialization of phytoplankton is different from Geider et al. (1997) which is used by the model (see above). Since the parameters of the model were unknown initially before the optimization procedure, the conversion using Geider et al. (1997) became complicated, and thus for simplicity it was not used. Zooplankton was taken as 10% of phytoplankton concentration in each depth (as in Lévy, 2015), since the NMP data does not provide depth resolution for zooplankton data. Detritus was taken from particulate organic carbon data of the NMP and converted to $mmol\text{-}N/m^3$ using the Redfield ratio. The initialization for all variables is equal throughout the Gulf domain, as we do not have observations from other parts of the Gulf.

2.3 Optimization

Model parameters were derived using a Genetic Algorithm (**GA**). GAs are widely used for optimization of dynamical models in general and specifically for NPZD models (e.g Rückelt et al., 2010; Schartau & Oschlies, 2003). The optimization was run on a simplified 1D offline model (only depth) in order to reduce computational time. Vertical eddy diffusivity values were read from the 3D physical model (KPP coefficients).

The algorithm creates 24 "chromosomes" in each generation, which contain a combination of the parameters in binary form. The next generation is composed partially by "mating" (combining half of each chromosome to a new one) of the best fits and partially by random "mutation" (changing one binary digit of the chromosome). The GA worked on 13 parameters for 600 generations in realistic ranges (as can be found in Table 1). The GA searches for the maximum fitness, which is the inverse of the cost function (error). If the GA converges and fitness does not differ by 20% from the previous generation, the model parameters are initialized from random values, while the best set of parameters are saved (elitism). The GA parameters are detailed in Table 2.

Monthly observations collected by the NMP during the period December 2010 to November 2012 were used for the optimization procedure. Depth profiles of chlorophyll and nitrogen (nitrate and nitrite) from Station A, as well as zooplankton in the upper 100 m, were used for the optimization algorithm. Nitrogen measurements are conducted using a quickchem 8000 flow injection analyzer, which is based on a color reaction with each specific reagent and is then analyzed by the machine's spectrophotometer. Chlorophyll is extracted and measured using a Fluorometer. Zooplankton is measured in the upper 100 m of the water column using a Bongo plankton net. The water is then filtered for different sizes and burnt. Difference in weight before and after the burning results in total biomass estimation. Zooplankton Ash Free Dry Weight (**AFDW**) is converted to organic carbon using 50% of the AFDW (Salonen et al., 1976).

The cost function (Equation 6) was composed of the vertical sum of the common logarithm of the squared errors for each of the variables - chlorophyll, nitrate and zooplankton, which are then summed up. The reasoning behind taking the logarithm is that the chlorophyll distribution is skewed. Thus, by taking the logarithm of chlorophyll, the distribution becomes less skewed and the squared error was then represented more correctly. We added a constant of 0.02 to all measurements to

Table 2. GA parameters used for optimization procedure.

GA Parameter	Description	Value
Precision	Number of values tested between range of parameters	10 bit or 1024 values
Chromosome length	Number of parameters to be optimized	13
Number of chromosomes	Number of sets of parameters	24
Number of generations	Number of generations to run the optimization	600
Probability for crossover	Probability to mate	0.5
Probability for mutation	Probability for mutation	0.01
Restart with elitism	Difference between all chromosome fitness is less than	20%

avoid zero values. This was then done to all the variables that were being optimized. Thus, the cost function was:

$$Cost = \sum_{l=1}^{L} \frac{1}{T} \sum_{j=1}^{T} \sum_{k=1}^{D} [log_{10}(\frac{C_{l,j,k}^{obs}}{\omega} + 0.02)^2 - log_{10}(\frac{C_{l,j,k}}{\omega}^{mod} + 0.02)^2] \quad (6)$$

Where $C_{l,j,k}$ is the compared variable l (CHL, N and Z) in time j and depth k. C^{obs} denotes the observation and C^{mod} denotes the model result. ω is a weight factor with same units as the compared variable, and was found after trial and error that the best suitable weight was one for all optimized variables. L is the number of variables optimized in the process and is equal to three. T is the number of observations (number of months) and D is the number of depths. Each variable was normalized to T. T is equal to 24 for chlorophyll and nitrogen and 21 for zooplankton, since these are the data available in the NMP. Zooplankton has a lower influence on the cost function because the cost function is not divided by the number of observations (zooplankton data is depth integrated). The cost function was constructed in this way since nitrogen and chlorophyll observations are more accurate than zooplankton data, which can represent also predators in higher trophic levels. The minimum cost function for the two years yielded a value of 1.6.

The optimized results for the same date and time of chlorophyll, nitrogen and zooplankton in a grid point closest to Station A are shown in Figures 6 middle row, 7 and 8 respectively. Figure 6 shows the optimization results of the 1D model (Upper panels), 3D model (middle panels) and the NMP observations (lower panels). The 1D 2011 modeled results show better agreement to observations compared with the 3D 2011 results. 1D 2012 optimized chlorophyll showed very high concentrations in the deep chlorophyll maximum during summer and very low concentrations during winter. 3D 2012 shows better resemblance to observations compared with 1D 2012, even though it does not simulate the large peak of chlorophyll in May. We estimate that this peak is missed due to a mixing event that was not simulated by the model, since it was missed in the NMP monthly observations (see Section 2.4 for more details).

Nitrogen (Figure 7) shows good resemblance to observations. It is apparent that in 2011 deep nitrogen is fairly constant in both model and observations, while nitrogen in the upper water column is scarce. 2012 also shows good resemblance, although the increase in nitrogen is more gradual during mixing months (January-March) in the observations compared with the model. Nitrogen in the deep water (under 200 m) increases in both model and observations gradually, however in the observations the increase is faster.

Modeled zooplankton peaks are in the same time of the NMP observations (∼April, Figure 8). Zooplankton values were higher than the observations both in

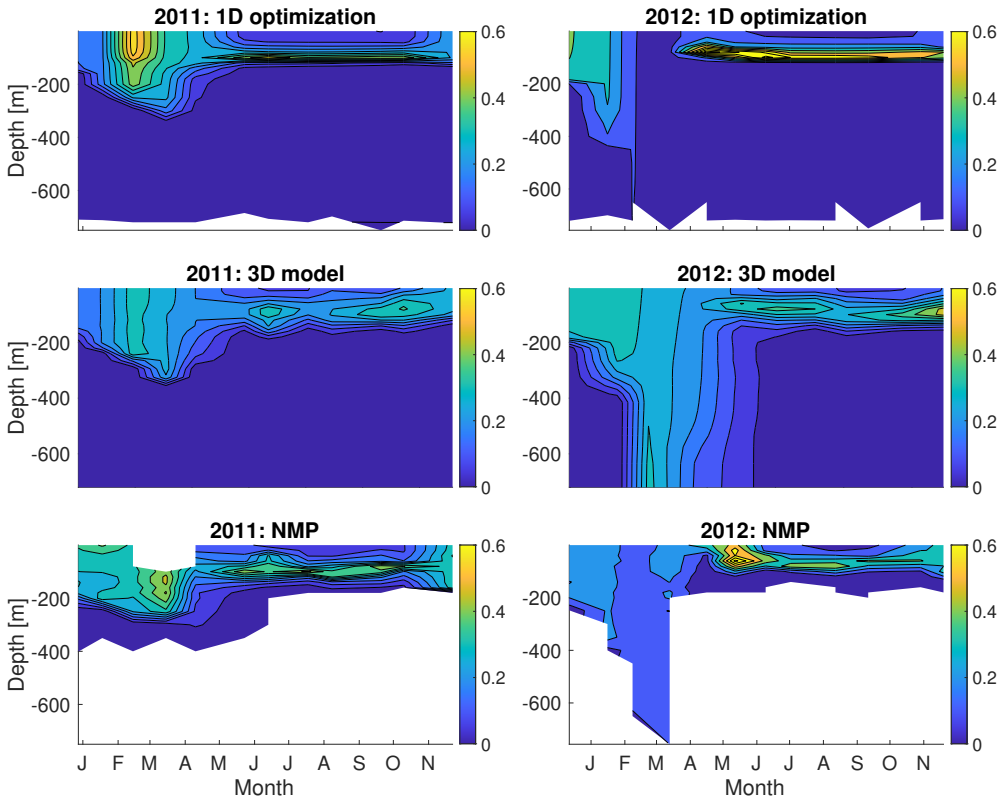

Figure 6. Optimization procedure for chlorophyll [$\mu g\text{-}chl/l$] in 2011 (left, shallow mixing) and 2012 (right, deep mixing). The upper row shows the 1D model after optimization. The middle row shows the final 3D model using the optimized parameters from the 1D optimization. The bottom row shows the NMP monthly observations.

April peaks (although in the range of observed values by the NMP) and during summer. Larger differences between simulated and observed zooplankton are expected compared with the other optimized variables due to zooplankton's lower contribution to the cost function (see explanation above).

2.4 Model comparison to independent data

The model was compared to three types of independent observations, for which the ecological parameters were not optimized for: (1) daily surface chlorophyll observations; (2) surface chlorophyll satellite data of MODIS-AQUA level 3 and (3) climatological conditions.

Surface chlorophyll is measured daily at a fixed location on the pier of the Underwater Observatory of Elat by the NMP (pier is illustrated in Figure 1). Chlorophyll is calculated from spectrophotometer measurements on water samples. These observations for 2011 and 2012 were compared to 2011 and 2012 simulated surface chlorophyll daily means in a grid point closest to Station A and can be seen in Figure 9. Pier chlorophyll has been shown to be lower than Station A surface chlorophyll by an average of 0.09 $\mu g/l$ (Zarubin et al., 2017). Simulated surface chlorophyll is lower compared with NMP observations, however the shape of the modeled surface chlorophyll is similar to that of the observations. Correlation be-

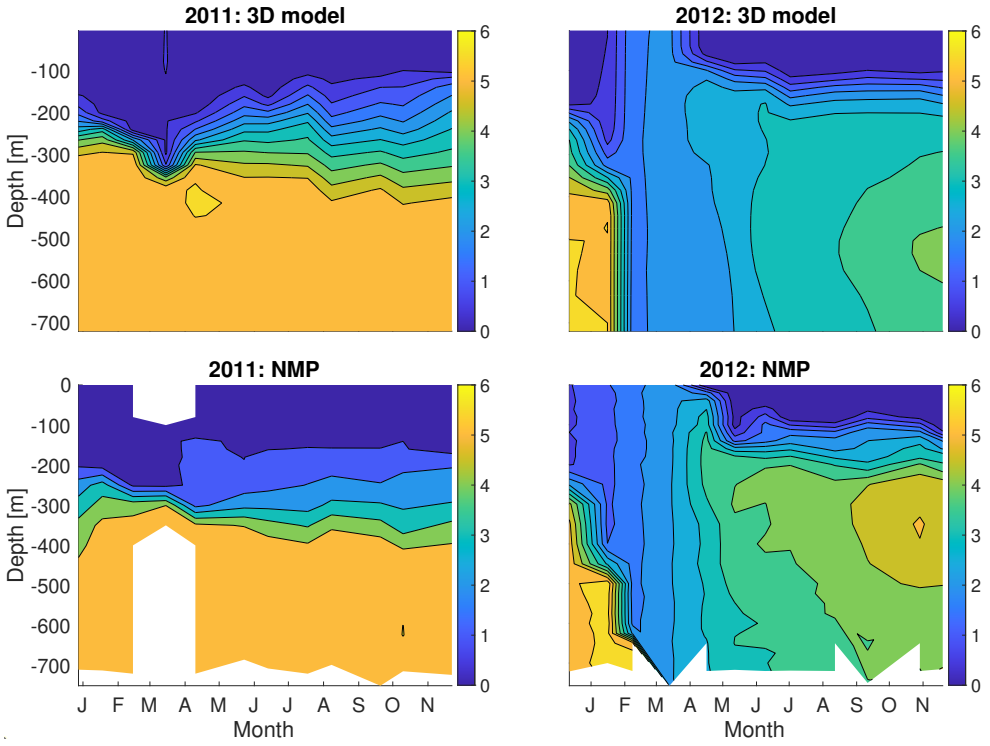

Figure 7. Simulated (upper panels) and observed (lower panels) nitrogen [$mmol\text{-}N/m^3$] in 2011 (left, shallow mixing) and 2012 (right, deep mixing).

tween the pier observations and simulation is R=0.44. The pier observations show a very strong bloom in 2012 which is divided into two parts. The second large peak (between April and May 2012) is not reproduced in its high magnitude by the simulations. The second peak might be missed due to a second mixing event not captured by the NMP observations. We compared SST daily observations to simulated SST (Figure 9) and found that there was a higher rapid temperature peak event in the beginning of April (22.5 ^{o}C) observed by the NMP compared with (21.8 ^{o}C) in simulations. This stratification event might have caused the increase in surface chlorophyll, which was not reproduced in its magnitude by the model.

We compared model results to surface chlorophyll from MODIS-AQUA level 3 (Figure 10). The comparison was done on the mean upper 50 m due to the optical depth of the satellite (as explained in `https://oceancolor.gsfc.nasa.gov/forum/oceancolor/topic_show.pl?tid=553`). The high surface chlorophyll concentration in winter is reconstructed by the model, while winter values are low in both model and satellite observations. Mixing season of 2012 shows the highest difference between model and observations, as the gradient in chlorophyll is less pronounced in the model compared with satellite data. These differences may be due to a stratification and mixing event in 2012 that was not simulated correctly by the model.

The climatological run was done using the physical model described in Biton and Gildor (2011b) and the optimized parameters found by the optimization procedure (Table 1). Although the model was not optimized for the climatological solution, which exhibit high variability in mixing depth throughout the years, the model reproduces many similarities to observations (see comparison in Berman & Gildor, in press).

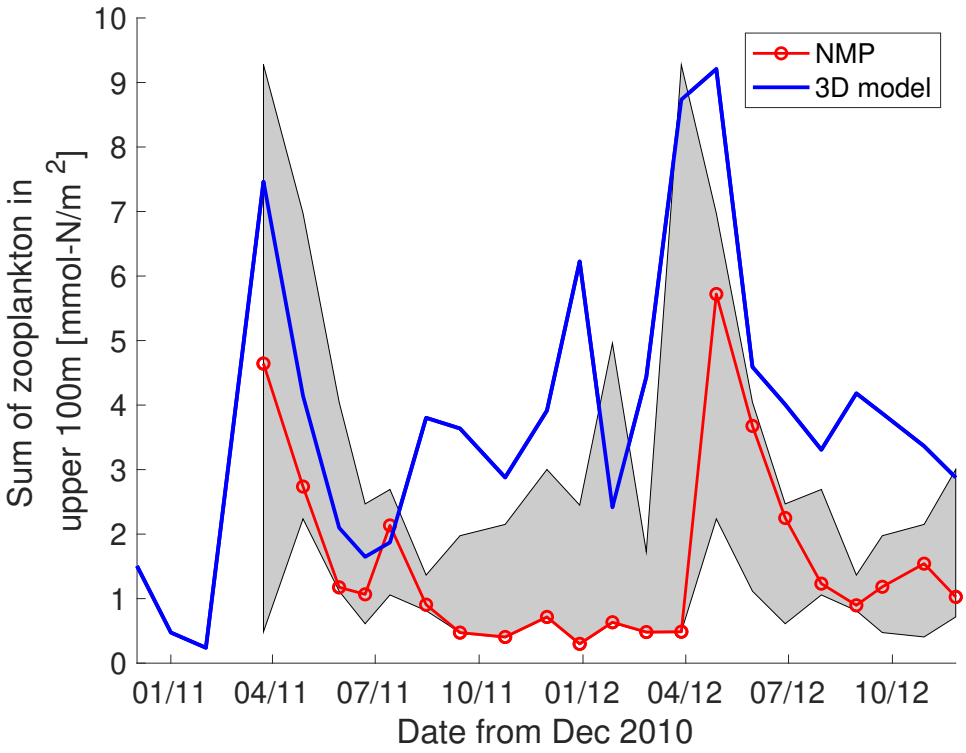

Figure 8. Observed (red) and simulated (blue) zooplankton integrated over the upper 100 m [$mmol\text{-}N/m^2$] in 2011 and 2012. Gray area represents the maximum and minimum monthly values measured by the NMP.

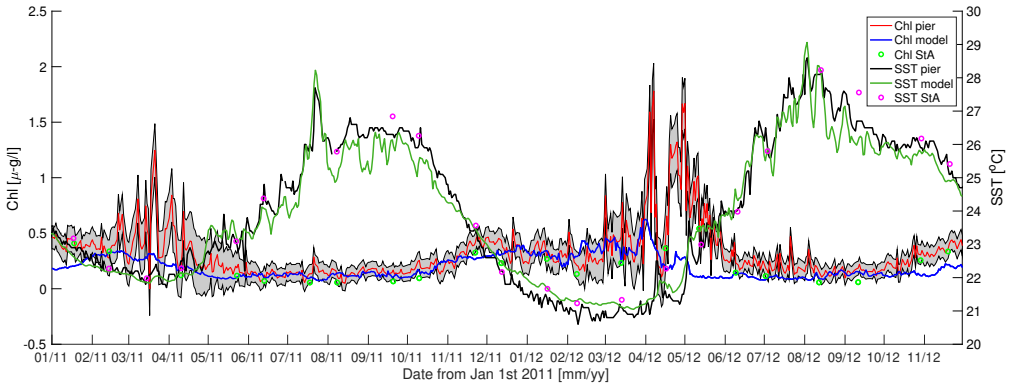

Figure 9. Observed and simulated daily surface chlorophyll and SST. Chlorophyll (red) and SST (black) observations were made at the pier of the Underwater Observatory of Elat by the NMP and are compared with the chlorophyll (green dots) and SST (magenta dots) measured in the surface in Station A by NMP. Simulated surface chlorophyll (blue) and SST (green) are compared to observations. Gray area is the standard deviation of chlorophyll calculated from all chlorophyll surface observations in the years 2004-2015 in the same day of year.

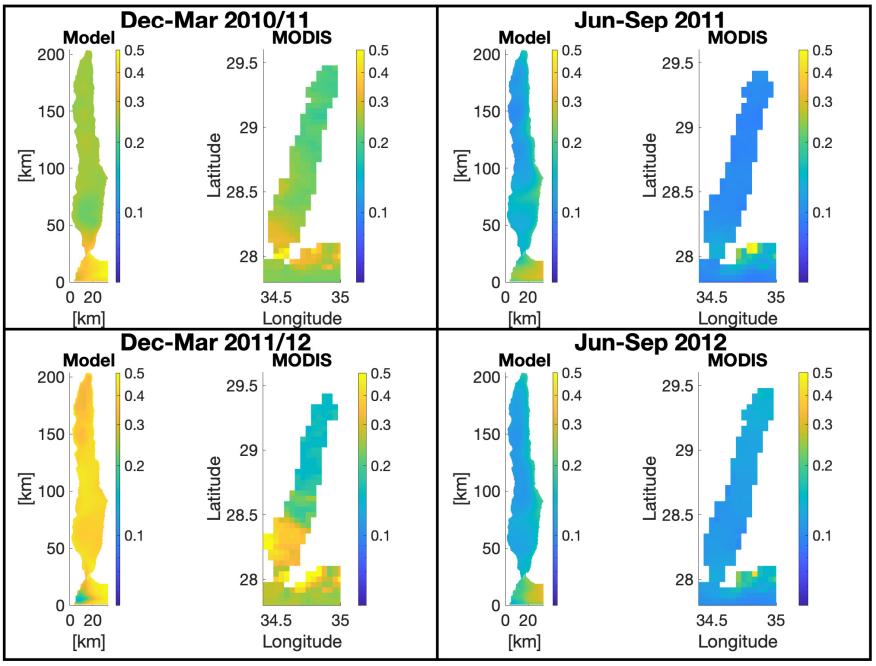

Figure 10. Surface chlorophyll $[\mu g/l]$ as observed by MODIS-AQUA level 3 imagery compared with model simulations mean over the stratified season (July-September) and mixed season (December-March) in 2011 and 2012.

3 Equations and definitions

3.1 Surface and integrated phytoplankton concentrations

We examined phytoplankton dynamics in the surface water and in the whole water column, using the following definitions:

Surface phytoplankton concentration $[mmol\text{-}N/m^3]$ was defined as the concentration in the upper layer of the model, which is 10 m deep. The results are insensitive to this specific depth and will yield the same conclusions when using the upper 35 m.

Integrated phytoplankton concentration $[mmol\text{-}N/m^2]$ is calculated as the phytoplankton depth integration over the whole water column, i.e. as $\Sigma_{i=1}^{n} P_i \Delta z_i$, where P_i is the phytoplankton concentration in each depth (z_i) and $n = 32$ is the number of grid points in the water column.

3.2 Phytoplankton rates

Surface and integrated phytoplankton specific rates of change $[1/d]$ are the measure of the change in phytoplankton concentration in every given time and location, which is affected by both ecological and physical processes, divided by phytoplankton concentration. We calculate various rates (as detailed below) to better understand the annual cycle of the ecological system and the bloom dynamics. Calculations of the integrated and surface specific rates are similar to Chiswell et al. (2015). The following defined rates are either surface or integrated rates, as detailed below. Note that the specific rates are somewhat different from the mass rates (not divided by the phytoplankton concentration) and thus do not exactly reconstruct

the surface and integrated phytoplankton concentration. However, we are interested in the change normalized to phytoplankton concentration.

Surface rate $[1/d]$ is the rate of change in the model upper layer, e.g. $\frac{1}{P_{i=1}}\frac{\partial P_{i=1}}{\partial t}$.

Depth integrated rate $[1/d]$ is the integrated rate over the whole water column. For example, the integrated net growth rate is calculated as: $\frac{1}{\Sigma_{i=1}^{n} P_i dz_i}\Sigma_{i=1}^{n}\frac{\partial P_i}{\partial t}\Delta z_i$, (Similar to Chiswell, 2011).

Growth rate $[1/d]$ is the rate in which phytoplankton grow while limited by both nutrients and light ($\frac{1}{P}\mu\frac{N}{N+k_{satN}}i_{lim}P$).

PAR limited growth rate $[1/d]$ is the growth rate if only light was limiting the growth ($\frac{1}{P}\mu i_{lim}P$).

N **limited growth rate** $[1/d]$ is the growth rate if only nutrients were limiting the growth ($\frac{1}{P}\mu\frac{N}{N+k_{satN}}P$).

Ecological growth rate $[1/d]$ is the sum of the ecological rates ($\frac{1}{P}(\mu\frac{N}{N+k_{satN}}i_{lim}P - g\frac{P^2}{P^2+k_{gsat}^2}Z - m_pP - m_{pn}P)$).

Physical rates $[1/d]$ is the sum of the advection and vertical mixing rates in the phytoplankton equation ($-\frac{1}{P}\vec{V}\vec{\nabla}P + \frac{1}{P}\frac{\partial}{\partial z}(K\frac{\partial P}{\partial z})$).

Net growth rate $[1/d]$, is the sum of all ecological and physical processes in the equation for P, Equation 2. The net growth rate is composed of the growth rate ($\frac{1}{P}\mu\frac{N}{N+k_{satN}}i_{lim}P$), mortality ($-\frac{1}{P}(m_p + m_{pn})P$), grazing ($-\frac{1}{P}g\frac{P^2}{P^2+k_{gsat}^2}Z$) and the physical rate ($-\frac{1}{P}\vec{V}\vec{\nabla}P + \frac{1}{P}\frac{\partial}{\partial z}(K\frac{\partial P}{\partial z})$). Net growth rate determines the phytoplankton concentration in the surface/integrated water column.

3.3 Nutrient rates

Ecological nutrient rate $[1/d]$ is the sum of the nutrient ecological rates (Equation 1, $\frac{1}{P}(-\mu\frac{N}{N+k_{satN}}i_{lim}P + k_{min}D + m_{zn}Z + m_{pn}P)$).

Physical nutrient rate $[1/d]$ is the sum of the advection and vertical mixing rates in the nutrient equation (Equation 1, $\frac{1}{P}(-\vec{V}\vec{\nabla}N + \frac{\partial}{\partial z}(K\frac{\partial N}{\partial z}))$).

Net nutrient rate $[1/d]$, is the sum of all ecological and physical processes in the nutrient equation (Equation 1, $\frac{1}{P}\frac{\partial N}{\partial t} = \frac{1}{P}(-\mu\frac{N}{N+k_{satN}}i_{lim}P + k_{min}D + m_{zn}Z + m_{pn}P - \frac{1}{N}\vec{V}\vec{\nabla}N + \frac{\partial}{\partial z}(K\frac{\partial N}{\partial z}))$).

3.4 Active mixed layer depth

The Active Mixed Layer Depth (**AMLD**) was calculated as the maximum depth where the eddy diffusion coefficient is larger than 10^{-2} m^2/s. For more details, see Berman and Gildor (in press).

3.5 Difference between the two years

Difference between the two years of deep and shallow mixing for the variables (phytoplankton concentration and rates) was calculated for the surface and integrated phytoplankton and AMLD in the following way. First, for each of these years we calculated the temporal mean of the variable between December to February. Then we computed the difference between them as: $Diff = C_{deep} - C_{shallow}$, where $Diff$ is the difference calculated, C_{deep} is the temporal mean variable in the year of deep mixing between December and February, and $C_{shallow}$ is the same variable in

the year of shallow mixing. Thus, if $diff$ is positive, the variable increased more in the year of deep mixing compared with the year of shallow mixing and vise versa. It is important to note here that the rates do not correspond exactly to the difference calculated for the phytoplankton concentration for two main reasons: 1) the concentration here takes into account the initial concentration in December, which is different between the two years. The rates however calculate how this difference has changed between December and February without taking into account the initial concentration; 2) the rates are normalized to phytoplankton concentration (either surface or integrated) in order to achieve specific rates. Due to the normalization, we see how the rates differ per phytoplankton cell and not how the sum of phytoplankton changes. Although the rates do not exactly represent what we see in the concentrations, they do represent the change in phytoplankton concentration between these months and since they are normalized they do not take the initial or high concentration into account. This way we can understand how the processes change between the years without concerning with the phytoplankton concentration change between the years.

3.6 Nutrient accumulation

To examine the nutrient accumulation in the deep water, we simulated the two years of shallow and deep mixing, and then ran the year of shallow mixing three more times. This allowed us to examine how the nutrients accumulated in depth during four years after the deep mixing (including the first summer after deep mixing). By summing up the nutrients ecological and physical rates under 400 m over a whole year since the mixing, we derive the relative contribution of each rate (physical or ecological) compared with the net nutrient rate. We note that the first year's contribution is taken between May-November (exactly after mixing), while the other years are calculated between December-November.

4 Results

The difference between surface and integrated phytoplankton and AMLD between the months December to February (Figure 11) shows significant changes between the years of deep and shallow mixing. Surface phytoplankton difference (Figure 11a) shows a small increase of surface phytoplankton in the north ($\sim$0.06 $mmol - N/m^3$) compared with a high increase in the south ($\sim$0.24 $mmol - N/m^3$). Integrated phytoplankton (Figure 11b) exhibits an inverse behavior, with a higher increase in the north ($\sim$90 $mmol - N/m^2$) compared with a low increase in the south ($\sim$20 $mmol - N/m^2$). AMLD difference (Figure 11c) corresponds to the integrated phytoplankton and shows that mixed layer deepening occurs more in the north ($\sim$300 m deeper in 2012), where stratification is weaker, compared with the southern Gulf ($\sim$0-50 m deeper in 2012).

Figure 12 shows the difference for the rates of surface phytoplankton. The difference of the surface net growth (Figure 12, right panel) shows negative values throughout the Gulf, however the spatial variability is high with very low rates in the north compared with the south (0 in the south and -0.018 $1/d$ in the north). As can be seen from the physical (Figure 12, left panel) and ecological rates (Figure 12, middle panel), the negative values in the north arise from a stronger negative physical rate compared with the ecological rate. In the surface water, the main physical process in this season which causes the physical rates to be negative is vertical mixing. Thus, as expected from the AMLD difference between the years (Figure 11c) we can see that where mixing is enhanced between the years, there is a stronger decrease in phytoplankton concentration. In the southern Gulf however, the differences are smaller, also mainly due to the mixing effect. Thus, we can see that stronger

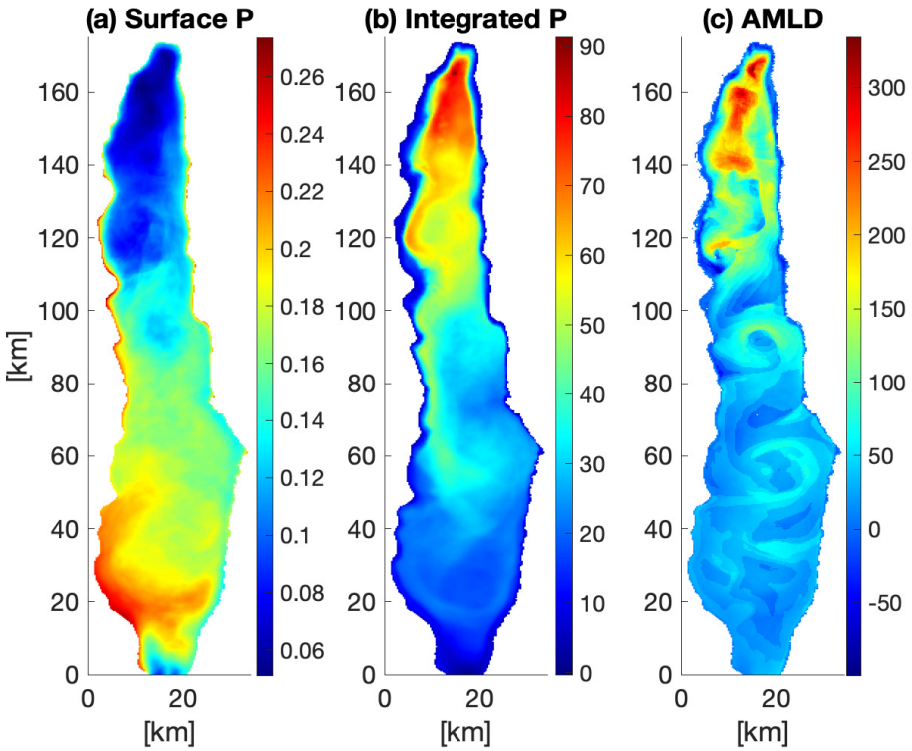

Figure 11. Difference between years of deep and shallow mixing of surface ($mmol\text{-}N/m^3$) and integrated ($mmol\text{-}N/m^2$) P and AMLD [m] shows spatial differences in the response of the Gulf to changes in mixing depth: (a) difference of surface P shows that in the year of deep mixing there is a higher concentration in the south compared with the north; (b) difference of integrated P shows that in the year of deep mixing there is an increase in the northern Gulf compared with the south; (c) AMLD difference shows that in the year of deep mixing there is a larger increase in the north compared with the south.

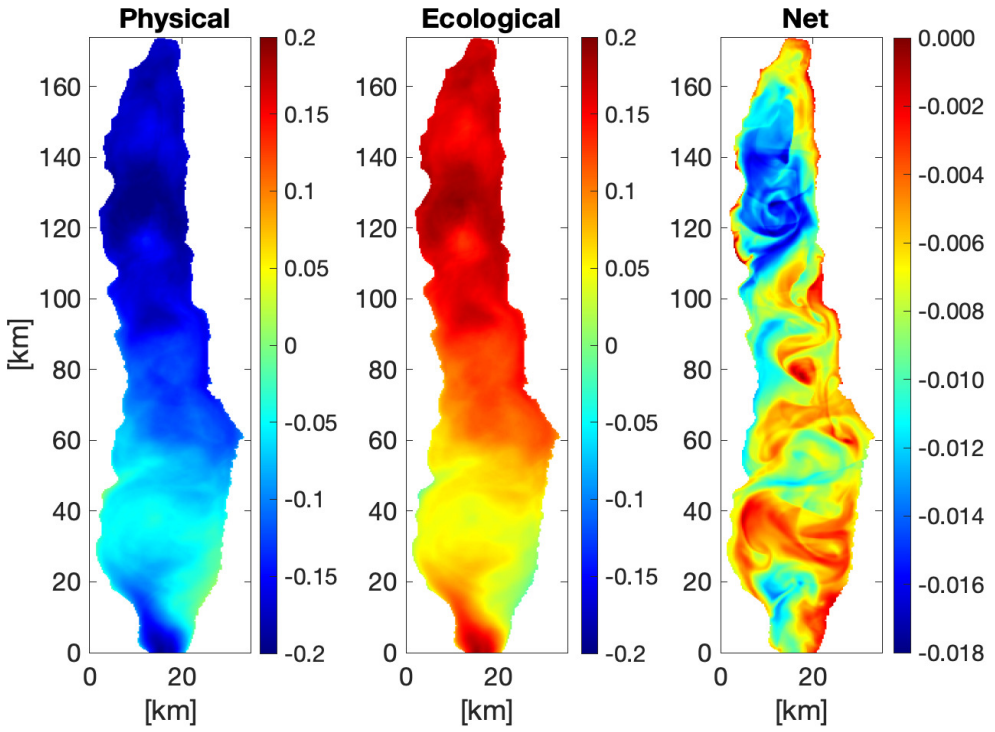

Figure 12. Difference of specific surface P rates of change $(1/d)$. Left panel - difference of surface physical rates. Middle panel - difference of surface ecological rates. Right panel - difference of surface net growth rate.

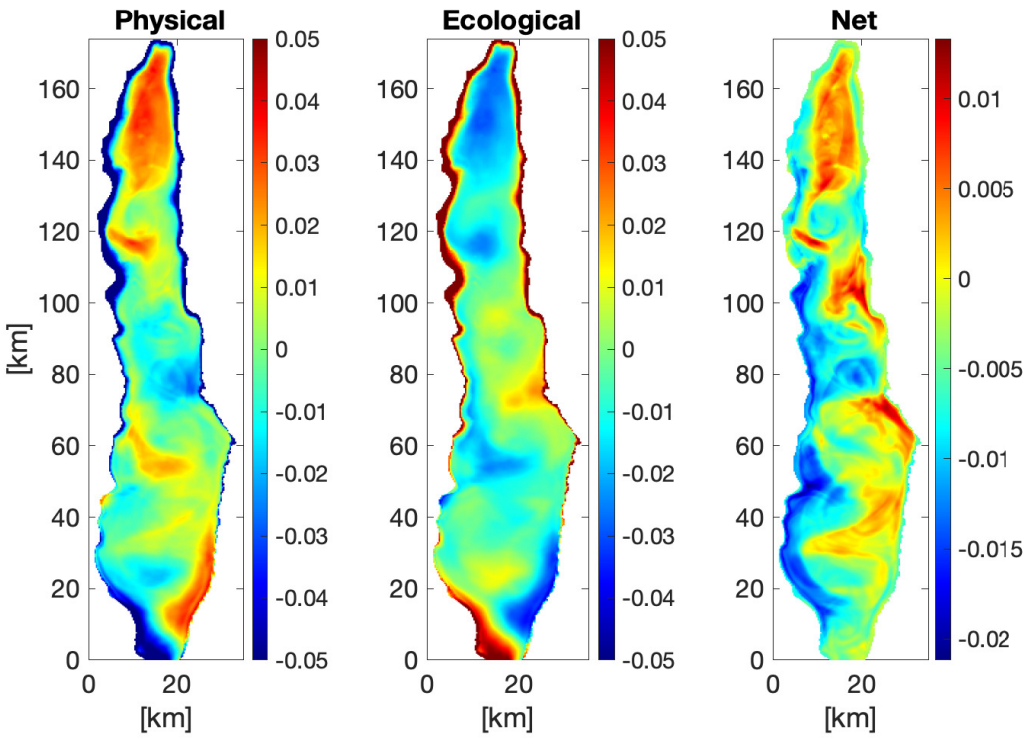

Figure 13. Difference of integrated P rates of change $[1/d]$. Left panel - difference of integrated physical rates. Middle panel - difference of integrated ecological rates. Right panel - difference of integrated net growth rate.

mixing conditions cause phytoplankton to decrease in the north more than in the south. Thus, the spatial variability in surface phytoplankton rates increased in years of deeper mixing.

Difference of net integrated phytoplankton rates (Figure 13, right panel) shows a high increase of integrated phytoplankton concentration in the north ($\sim$0.01 $1/d$). The physical processes dominate the northern Gulf. This can be seen from the sign of the processes, where the difference of the physical rates is positive (Figure 13, left panel) in the north. However, unlike the surface net growth, in the integrated column vertical mixing vanishes when integrating over the whole water column, leaving horizontal advection as the process responsible for the change. Thus, we found that the importance of horizontal advection for the northern integrated phytoplankton concentration is enhanced with deep mixing. The center and southern parts of the Gulf also show areas of high increase, especially close to the eastern shore ($\sim$0.01 $1/d$). This is due to a combination of the physical and ecological processes. Some areas show a positive effect for both the physical and ecological processes, while in other areas the processes work in opposite signs. The difference between the years in the integrated specific net growth rate in the center and southern Gulf was not visible from the phytoplankton concentration (Figure 11).

Limitation of light and nutrients on phytoplankton growth rate have been tested using light and nutrient limited growth (as described in Section 3). Figure 14 shows the nutrient limited, light limited and light and nutrient limited growth (growth rate) differences for surface phytoplankton. Since growth rate difference (Figure 14, left panel) is almost identical to N limited growth differences (Figure 14,

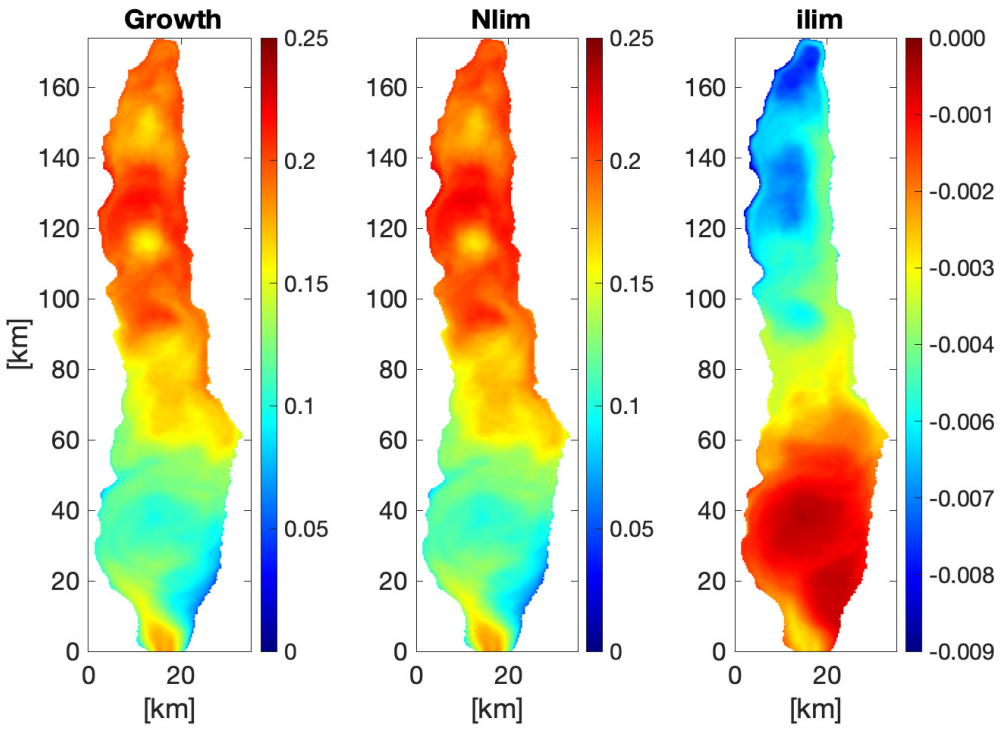

Figure 14. Difference of light and nutrient limitation on surface growth rate $[1/d]$. Left panel: surface growth rate. Middle panel: surface N limited growth. Right panel: surface light limited growth. It is apparent that the difference of nutrient limited growth is almost identical to the growth rate difference, thus concluding that the surface is limited by nutrients in both year of deep and shallow mixing.

middle panel) we concluded that nutrients are the only limiting factor in the surface waters and this is preserved even in years of deep mixing when vertical mixing provides higher nutrient concentration to the surface. Since the difference in light limitation (Figure 14, right panel) was very low between the years (maximum absolute difference of $\sim$0.01 $1/d$), it did not affect the growth, and nutrients are the limiting factor even when mixing increases the amount of nutrients in the surface.

As opposed to the surface rates, the limitation on integrated growth (Figure 15) in the northern Gulf is due to light limitation. Due to a decrease in light limitation (Figure 15, right panel) in the northern Gulf (of $\sim$-0.02 $1/d$ since mixing is deeper), the integrated growth rate in the northern Gulf is limited by light in the north, even though nutrient limited growth would have resulted in higher phytoplankton growth (Figure 15 middle panel). The southern Gulf however is not as affected by the light limitation. This is in correspondence with the difference in the AMLD between the northern and southern Gulf in the two years.

Nutrient accumulation in depth (under 400 m) in Station A in the northern Gulf was tested. The model reproduces the nutrient concentration for 2011 and 2012 as used above, and was further run for three more years of shallow mixing (as detailed in Section 3). The first year was most dominant in reconstructing the deep nutrient concentration in both observations and model, as the nutrient concentration increased in a high rate at this year from $\sim$1.8 $mmol\text{-}N/m^3$ to $\sim$4 $mmol\text{-}N/m^3$. In the first year of shallow mixing nutrients increased by $\sim$0.6 $mmol\text{-}N/m^3$, in the

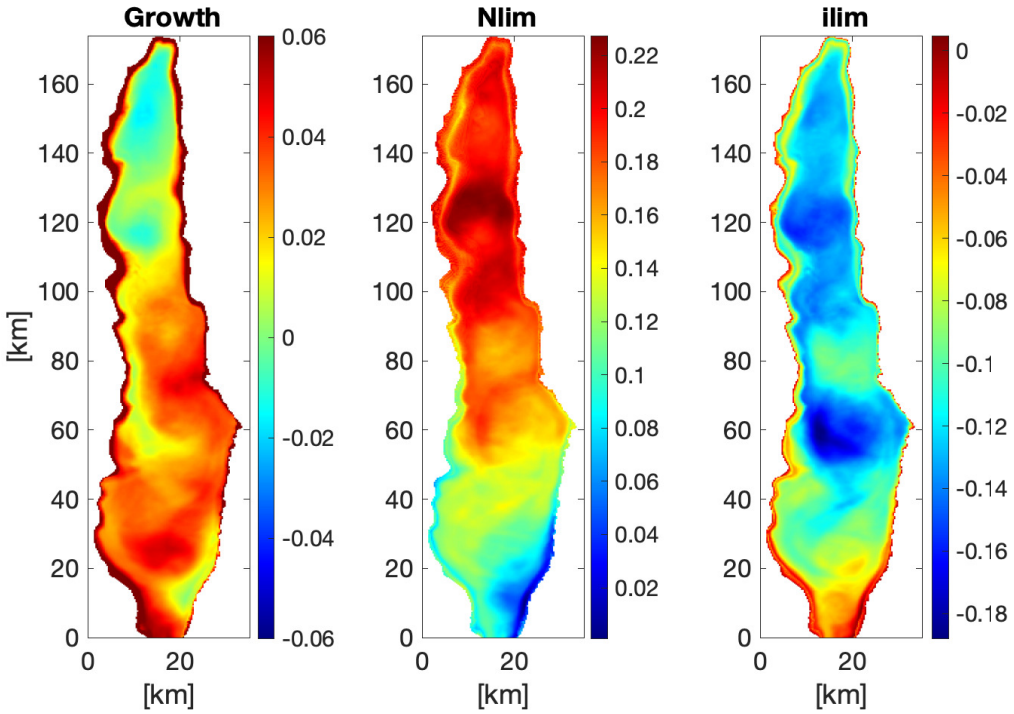

Figure 15. Difference of light and nutrient limitation on integrated growth rate $[1/d]$. Left panel: integrated growth rate. Middle panel: integrated N limited growth. Right panel: integrated light limited growth. Here, growth rate limitation is a combination of both nutrient and light limited growth rates. However, it is apparent that the northern Gulf is limited by light, since the difference in growth rate there is negative even though N limited growth is positive there.

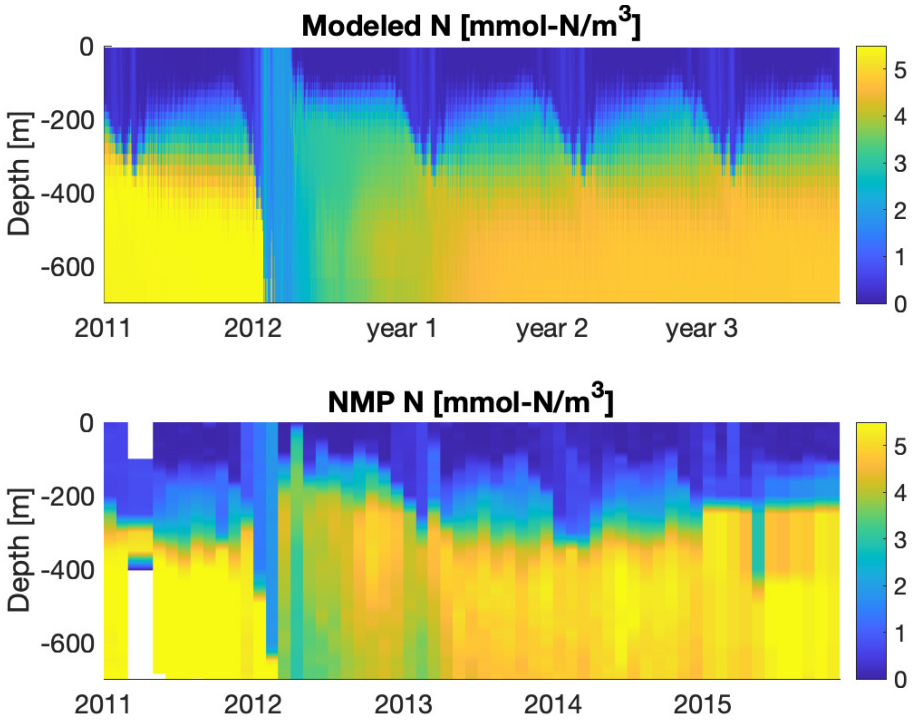

Figure 16. Nutrient accumulation in depth after a year of deep mixing in Station A. Upper panel: modeled N in Station A in 2011 and 2012, and three more years of shallow mixing. Lower panel: observed N by the NMP in Station A between the years 2011-2015. The decrease in deep N (under 400 m) is apparent in 2012 in both model and observations. After the mixing, there is a gradual increase in deep N concentration.

second year by $\sim$0.1 $mmol\text{-}N/m^3$ and in the third by $\sim$0.02 $mmol\text{-}N/m^3$. The maximum nutrient concentration in the northern deep water in the model however at the end of the accumulation period does not reach the maximum value in the NMP observations (model maximum 4.8 $mmol\text{-}N/m^3$ and observations maximum 5.6 $mmol\text{-}N/m^2$).

The integrated rates under 400 m showed that the accumulation in 2012 was 60% by physical processes and only 40% by ecological processes. In the first year of shallow mixing it was 50% by ecological processes and 50% by physical processes. In the second year it was 60% by ecological processes and 40% by physical processes. In the last year 100% of the accumulation was due to ecological processes, but it is important to note that the increase in nutrients in the last year was very small, as detailed above. Thus, we found that the largest increase of deep nutrients in the Gulf after mixing was mainly due to physical processes, and this decreased as the years progressed. The effect of the physical processes reduced as the years progressed, since the Gulf's deep water became more homogenous and spatial differences in the deep layer were less apparent. This caused horizontal advection to decrease in the deep water, and thus physical processes were less important for nutrient accumulation.

5 Discussion

We constructed the first 3D coupled physical-biological model optimized specifically for the Gulf. Previous coupled physical-ecological models for the Gulf included only one dimension, thus were not able to simulate numerous processes, such as the effects of advection (e.g. Kuhn et al., 2018). The model is optimized to nutrients, chlorophyll and zooplankton observations in Station A. Comparison to other observations which the model was not optimized for, including remotely-sensed surface chlorophyll, climatological conditions in the Gulf (used previously by Berman & Gildor, in press) and daily surface chlorophyll also give reasonable results. The main differences between the model and observations are probably due to a stratification/mixing event that was not simulated in its full magnitude by the model in the year of deep mixing due to the coarse temporal resolution of the observations.

The AMLD increased more in years of deep mixing in the northern Gulf compared with the south. Such spatial variability in the AMLD between the northern and southern Gulf has been reported previously (Paldor & Anati, 1979; Levanon-Spanier et al., 1979; Berman & Gildor, in press), and is due to the stronger southern stratification. However, further study should examine why this spatial variability is enhanced in years of deep mixing.

Surface net growth decreased in the northern Gulf in the year of deep mixing due to enhanced vertical mixing. The integrated growth increased in the north due to physical processes as well, however unlike in the surface, the integrated column physical processes include only horizontal advection. The effect of horizontal advection on integrated phytoplankton concentration in the northern Gulf was enhanced in years of deep mixing. This extends Berman and Gildor (in press)'s finding that deep mixed phytoplankton is advected from the south, and shows that as mixing depth increases, phytoplankton advection increases. The integrated net growth also showed an increase in the center and south of the Gulf, closer to the eastern shore. Coastal upwelling has been suggested to be a mechanism for elevated phytoplankton in the east coast of the Gulf (Labiosa et al., 2003). Increased coastal upwelling in years of deep mixing (due to increased winds) could potentially explain this phenomenon, but this should be tested in future work.

A possible explanation for the increased influence of advection on phytoplankton concentration can be derived from internal hydraulics theory. Mean surface buoyancy flux over the whole basin (which controls the AMLD) is linked to the exchange flow in a semi-enclosed basin through the straits (Ivey, 2004). When the buoyancy flux increases (due to increased cooling), so does the exchange flow into a semi enclosed basin, and thus the advection in the basin. This theory should be tested quantitatively in future work.

Nutrients were found to be the limiting factor for phytoplankton growth in the surface in both years. This is in agreement with Meeder (2012); Zarubin et al. (2017); Berman and Gildor (in press). We found that even in years of deep mixing where nutrients were very abundant in the surface, further nutrient increase would still promote phytoplankton growth.

We found that the effect of light limitation on the integrated growth rate increased when AMLD increased. This finding is intuitive, as deep mixing can cause phytoplankton to spend less time in the photic zone. We are in agreement with Berman and Gildor (in press) and Meeder (2012) that light does limit phytoplankton growth in areas of deep mixing, and show that the limitation increases with increased mixing. Our findings disagree with Zarubin et al. (2017); Stambler (2006) who claim that light does not limit phytoplankton growth in the Gulf.

Nutrient accumulation in depth was found to be more affected by physical processes (mostly by advection) in the year of deep mixing. This might explain why Kuhn et al. (2018) were not able to reconstruct the high nutrient concentration in depth in their 1D model, which lacks horizontal advection. However, we also found that in the third year of shallow mixing, the ecological processes dominated the accumulation of nutrients. Thus, after a few years of shallow mixing, physical processes are less important for deep nutrient accumulation.

We stress that the model does not simulate 2012's second mixing event in its full magnitude, thus model results are different from observations. Future work should examine: (1) the mechanism for the increased spatial variability in the deep mixed year; (2) the increased horizontal advection in the year of deep mixing and (3) the mechanism for increased integrated chlorophyll in the eastern Gulf in the year of deep mixing and

Appendix A Atmospheric model

Winds for the specific years of 2011 and 2012 were derived using the WRF (Weather Research and Forecasting, `http://www.wrf-model.org/index.php`) model. This work was part of a project funded by the Israel Park and Nature Reserve. The model domain consists of the Red Sea (260km x 520km), with 3 horizontal domains of varying resolutions, with the finest resolution of 1.3km, and 31 vertical levels. National Centers for Environmental Prediction (NCEP; details can be found on the homepage `http://www.ucar.edu/datasets/ds083/`) data was used for the initial and boundary conditions. Boundary layer height was resolved using the Yonsei University (YSU) PBL scheme (Hong et al. 2006). The model configuration resolved wind, transport and dry decomposition. Hourly winds for the two years were saved and used for the oceanographic model.

Acknowledgments

We thank Dr. Yael Amitai for technical help with the ocean simulations. HB thanks the Eshkol foundation administered by the Israel Ministry of Science and Technology (MOST) for providing her PhD fellowship under grant number 0399587. Additional travel funding was provided to HB by the Mediterranean Sea Research Center of Israel. We would like to thank the Israel National Monitoring Program of the Gulf of Elat (NMP) and NASA's Moderate-resolution Imaging Spectroradiometer (MODIS) for data provided to conduct this study.

References

Behrenfeld, M. J., & Boss, E. S. (2018). Student's tutorial on bloom hypotheses in the context of phytoplankton annual cycles. *Global Change Biology*, *24*(1), 55-77. doi: 10.1111/gcb.13858

Berman, H., & Gildor, H. (in press). Phytoplankton bloom in the Gulf of Elat/Aqaba: Physical vs. ecological forcing. *Journal of Geophysical Research*.

Biton, E., & Gildor, H. (2011a). The coupling between exchange flux through a strait and dynamics in a small convectively driven marginal sea: The Gulf of Aqaba (Gulf of Eilat). *Journal of Geophysical Research*, *116*(C6), 10.1029/2011JC006944.

Biton, E., & Gildor, H. (2011b). The general circulation of the Gulf of Aqaba (Gulf of Eilat) revisited: The interplay between the exchange flow through the Straits of Tiran and surface fluxes. *Journal of Geophysical Research*, *116*(C8), 10.1029/2010JC006860.

Biton, E., & Gildor, H. (2011c). Stepwise seasonal restratification and the evolution

of salinity minimum in the Gulf of Aqaba (Gulf of Eilat). *Journal of Geophysical Research*, *116*(C8), 10.1029/2011JC007106.

Biton, E., & Gildor, H. (2016). On the origin of a chain of eddies in the Gulf of Eilat/Aqaba. *Journal of Physical Oceanography*, *46*(8), 2269 - 2284. doi: 10.1175/JPO-D-15-0208.1

Biton, E., Silverman, J., & Gildor, H. (2008). Observations and modeling of a pulsating density current. *Geophysical Research Letters*, *35*(14), 10.1029/2008GL034123.

Capone, D. G., Bronk, D. A., Mulholland, M. R., & Carpenter, E. J. (2008). *Nitrogen in the marine environment*. Burlington, MA: Elsevier.

Carlson, D., Fredj, E., & Gildor, H. (2014). The annual cycle of vertical mixing and restratification in the northern Gulf of Eilat/Aqaba (Red Sea) based on high temporal and vertical resolution observations. *Deep Sea Research*, *84*, 1–17.

Chiswell, S. M. (2011). Annual cycles and spring blooms in phytoplankton: Don't abandon Sverdrup completely. *Marine ecology progress series*, *443*, 39–50.

Chiswell, S. M., Calil, P. H., & Boyd, P. W. (2015). Spring blooms and annual cycles of phytoplankton: A unified perspective. *Journal of Plankton Research*, *37*(3), 500-508. doi: 10.1093/plankt/fbv021

Dishon, G., Dubinsky, Z., Caras, T., Rahav, E., Bar-Zeev, E., Tzubery, Y., & Iluz, D. (2012). Optical habitats of ultraphytoplankton groups in the Gulf of Eilat (Aqaba), Northern Red Sea. *International journal of remote sensing*, *33*(9), 2683–2705.

Evans, G. T., & Garçon, V. C. (1997). *One-dimensional models of water column biogeochemistry*. Report of a Workshop held in Toulouse, France; November-December 1995.

Fennel, K., Losch, M., Schröter, J., & Wenzel, M. (2001). Testing a marine ecosystem model: Sensitivity analysis and parameter optimization. *Journal of Marine Systems*, *28*(1), 45–63.

Fennel, K., Wilkin, J., Levin, J., Moisan, J., O'Reilly, J., & Haidvogel, D. (2006). Nitrogen cycling in the Middle Atlantic Bight: Results from a three-dimensional model and implications for the North Atlantic nitrogen budget. *Global Biogeochemical Cycles*, *20*(3).

Follows, M. J., Dutkiewicz, S., Grant, S., & Chisholm, S. W. (2007). Emergent biogeography of microbial communities in a model ocean. *Science*, *315*(5820), 1843–1846.

Franks, P. J. S. (2002). NPZ models of plankton dynamics: Their construction, coupling to physics, and application. *Journal of Oceanography*, *58*(2), 379–387.

Geider, R. J., MacIntyre, H. L., & Kana, T. M. (1997). Dynamic model of phytoplankton growth and acclimation: Responses of the balanced growth rate and the chlorophyll a: carbon ratio to light, nutrient-limitation and temperature. *Marine Ecology Progress Series*, *148*, 187–200.

Genin, A., Lazar, B., & Brenner, S. (1995). Vertical mixing and coral death in the Red-Sea following the eruption of Mount-Pinatubo. *Nature*, *377*, 507–510.

Ivey, G. (2004). Stratification and mixing in sea straits. *Deep Sea Research*, *51*(4-5), 441–453.

Kuhn, A. M., Fennel, K., & Berman-Frank, I. (2018). Modelling the biogeochemical effects of heterotrophic and autotrophic N_2 fixation in the Gulf of Aqaba (Israel), Red Sea. *Biogeosciences*, *15*(24), 7379–7401.

Kuhn, A. M., Fennel, K., & Mattern, J. P. (2015). Model investigations of the North Atlantic spring bloom initiation. *Progress in Oceanography*, *138*, 176–193.

Labiosa, R. G., Arrigo, K. R., Genin, A., Monismith, S. G., & van Dijken, G. (2003). The interplay between upwelling and deep convective mixing in determining the seasonal phytoplankton dynamics in the Gulf of Aqaba: Evidence from SeaWiFS and MODIS. *Limnology and oceanography*, *48*(6), 2355–2368.

Large, W. G., Danabasoglu, G., Doney, S. C., & McWilliams, J. C. (1997). Sensi-

tivity to surface forcing and boundary layer mixing in a global ocean model: Annual-mean climatology. *Journal of Physical Oceanography*, *27*(11), 2418–2447.

Levanon-Spanier, I., Padan, E., & Reiss, Z. (1979). Primary production in a desert-enclosed sea—the Gulf of Elat (Aqaba), Red Sea. *Deep Sea Research*, *26*(6), 673–685.

Lévy, M. (2015). Exploration of the critical depth hypothesis with a simple NPZ model. *ICES Journal of Marine Science*, *72*(6), 1916-1925. doi: 10.1093/icesjms/fsv016

Marshall, J., Adcroft, A., Hill, C., Perelman, L., & Heisey, C. (1997). A finite-volume, incompressible Navier Stokes model for studies of the ocean on parallel computers. *Journal of Geophysical Research*, *102*(C3), 5753–5766.

Marshall, J., Hill, C., Perelman, L., & Adcroft, A. (1997). Hydrostatic, quasi-hydrostatic, and nonhydrostatic ocean modeling. *Journal of Geophysical Research*, *102*(C3), 5733-5752.

Meeder, E. (2012). *Dynamics of nitrogen species in the oceanic water column* (Unpublished doctoral dissertation). The Hebrew University of Jerusalem.

Paldor, N., & Anati, D. A. (1979). Seasonal variations of temperature and salinity in the Gulf of Elat (Aqaba). *Deep Sea Research*, *26*(6), 661 - 672. doi: https://doi.org/10.1016/0198-0149(79)90039-6

Rückelt, J., Oschlies, A., & Slawig, T. (2010). *Optimization of parameters and initialvalues in a marine npzd-type ecosystem model* (Vol. 1013) [Research Report]. Kiel, Germany: Institut für Informatik.

Salonen, K., Sarvala, J., Hakala, I., & Viljanen, M.-L. (1976). The relation of energy and organic carbon in aquatic invertebrates 1. *Limnology and oceanography*, *21*(5), 724–730.

Schartau, M., & Oschlies, A. (2003). Simultaneous data-based optimization of a 1D-ecosystem model at three locations in the North Atlantic: Part I— Method and parameter estimates. *Journal of Marine Research*, *61*(6), 765–793.

Smagorinsky, J. (1963). General circulation experiments with the primitive equations: I. The basic experiment. *Monthly weather review*, *91*, 99-164.

Stambler, N. (2006). Light and picophytoplankton in the Gulf of Eilat (Aqaba). *Journal of Geophysical Research*, *111*(C11), 10.1029/2005JC003373.

Suggett, D. J., Stambler, N., Prasil, O., Kolber, Z., Quigg, A., Vazquez-Dominguez, E., ... Berman-Frank, I. (2009). Nitrogen and phosphorus limitation of oceanic microbial growth during spring in the Gulf of Aqaba. *Aquatic microbial ecology*, *56*(2-3), 227–239.

Sverdrup, H. U. (1953). On conditions for the vernal blooming of phytoplankton. *Journal du Conseil*, *18*(3), 287–295.

Wolf-Vecht, A., Paldor, N., & Brenner, S. (1992). Hydrographic indications of advection/convection effects in the Gulf of Elat. *Deep Sea Research*, *39*(7), 1393–1401.

Zarubin, M., Lindemann, Y., & Genin, A. (2017). The dispersion-confinement mechanism: Phytoplankton dynamics and the spring bloom in a deeply-mixing subtropical sea. *Progress in oceanography*, *155*, 13–27.